a-PET and Weakened Triplet−Triplet Annihilation Self-Quenching Effects in Benzo-21-Crown-7-Functionalized Diiodo-BODIPY

Jifu Sun,* Weixu Li, Yuqi Hou, Xue Zhang, Zhongzheng Gao, Bo Wang,* and Jianzhang Zhao*

Read Online

| ACCESS | | Metrics & More | | Article Recommendations | | Supporting Information |

ABSTRACT: Weakening the triplet−triplet annihilation (TTA) self-quenching effect induced by sensitizers remains a tremendous challenge due to the very few investigations carried out on them. Herein, benzo-21-crown-7 (**B21C7**)-functionalized 2,6-diiodo-1,3,5,7-tetramethyl-8-phenyl-4,4-difluoroboradiazaindacene (**DIBDP**) was synthesized to investigate the influences of huge bulks and electron-rich cavities of **B21C7** moieties on the fluorescence emission and triplet-state lifetimes of **DIBDP** moieties. Density functional theory (DFT)/time-dependent DFT (TDDFT) computable results preliminarily predicted that **B21C7**

moieties had influences on the fluorescence emissions of **DIBDP** moieties but not on their localization of triplet states of **B21C7**-functionalized **DIBDP** (**B21C7-DIBDP**). The UV−vis absorption spectra, fluorescence emission spectra, and cyclic voltammograms verified that there was an electron-transfer process from the **B21C7** moiety to the **DIBDP** moiety in **B21C7-DIBDP**. However, the calculated results of ΔG_{CS} and E_{CS} values and nanosecond time-resolved transient absorption spectra demonstrated that the electron-transfer process from the **B21C7** moiety to the **DIBDP** moiety in **B21C7-DIBDP** had direct influences on the fluorescence emission of **DIBDP** moieties but not on the triplet states of **DIBDP** moieties. The experimental values of triplet-state lifetimes of **B21C7-DIBDP** were obviously longer than those of **DIBDP** at a high concentration (1.0×10^{-5} M); however, the fitted values of intrinsic triplet-state lifetimes of **B21C7-DIBDP** were slightly greater than those of **DIBDP** in the same solvent. These results demonstrated that the steric hindrance of **B21C7** moieties could weaken the TTA self-quenching effect of **DIBDP** moieties at a high concentration and the a-PET effect induced a proportion of the produced singlet states of **DIBDP** moieties and could not emit fluorescence in the form of radiation transition but they could be transformed into triplet states through intersystem crossing (ISC) processes due to the iodine atoms in the **DIBDP** moiety. The stronger a-PET effects in polar solvents induced smaller fluorescence quantum yields so that more singlet states of **DIBDP** moieties were transformed into triplet states to weaken the TTA self-quenching effects.
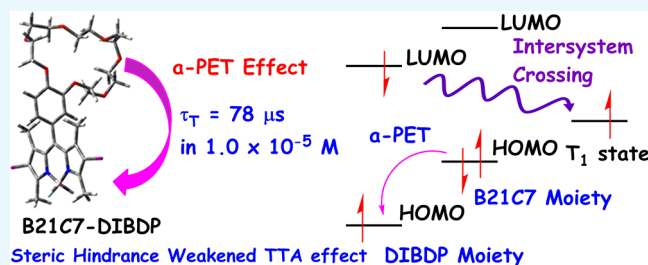
1. INTRODUCTION

Triplet photosensitizers have demonstrated a strong potential for a broad range of applications in numerous areas, such as photocatalysis,[1−7] photodynamic therapy (PDT),[8−19] photo-electric devices,[20−22] organic room-temperature phosphorescence (RTP) materials,[23−30] and triplet−triplet annihilation (TTA) upconversion.[31−41] Significantly, to complete the triplet−triplet energy-transfer (TTET) processes from photosensitizers to acceptors following the Dexter energy-transfer mechanism in most of these applications, the photosensitizers and acceptors must diffuse within a distance smaller than the Dexter radius (usually 0−1 nm) before the total triplet states of the sensitizers decaying;[31,35,36] therefore, a long-enough triplet excited-state is pivotal for a perfect photosensitizer besides the abilities of strong absorption of visible light and efficient intersystem crossing (ISC).[1,6,7,14,31,37,38,40] The triplet-state lifetimes of sensitizers can be influenced by many factors, and previous efforts have been devoted to prolonging their triplet-state lifetimes.[1,6,7,40,42−50] However, limited by the repulsive aggregation-caused quenching (ACQ) effect of the π-conjugated-system-containing and planar rigid sensitizers

(e.g., 2,6-diiodo-1,3,5,7-tetramethyl-8-phenyl-4,4-difluorobora-diazaindacene (**DIBDP**)),[51,52] the TTA self-quenching effect induced by these photosensitizers will cause additional lifetime quenching in the decaying of their transient absorption accompanied by their concentration increase, which will result in the experimental values of the triplet-state lifetimes to be much shorter than their intrinsic values in most cases due to the TTA self-quenching effects.[47,49−51] Although we have reported that huge bulks of pillar[5]arene moieties in **DIBDP**-functionalized pillar[5]arene could weaken the TTA self-quenching effect of **DIBDP** moieties,[51] owing to only one report, weakening the photosensitizers' TTA self-quenching effect is still a great challenge for their further applications.

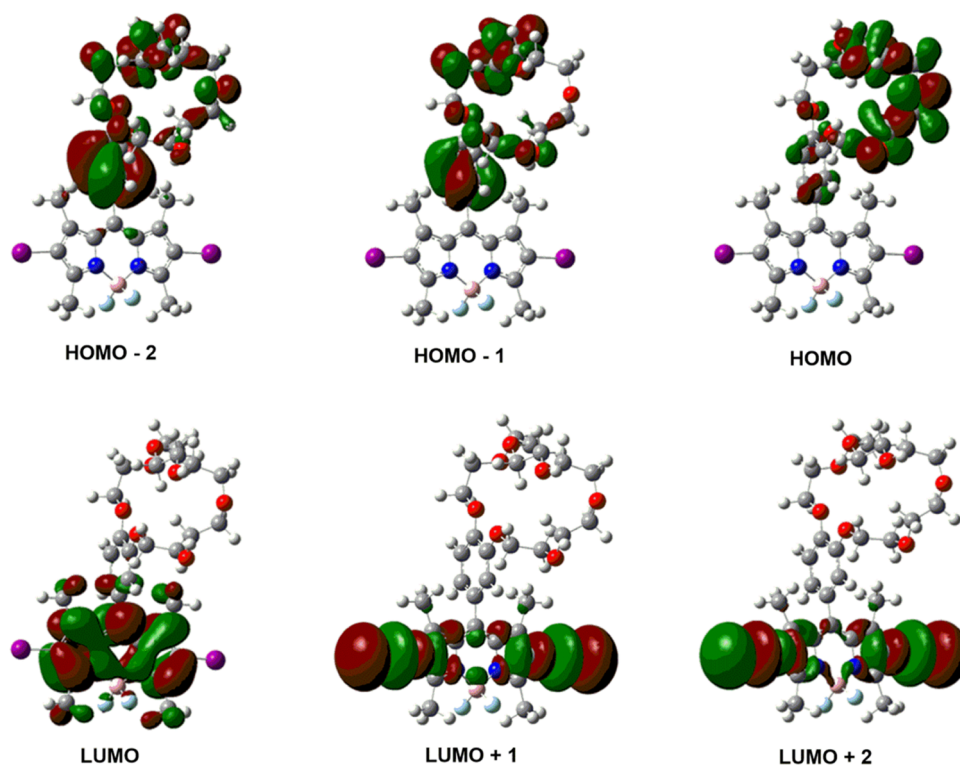**Scheme 1. Synthetic Routes of B21C7-DIBDP[a]**
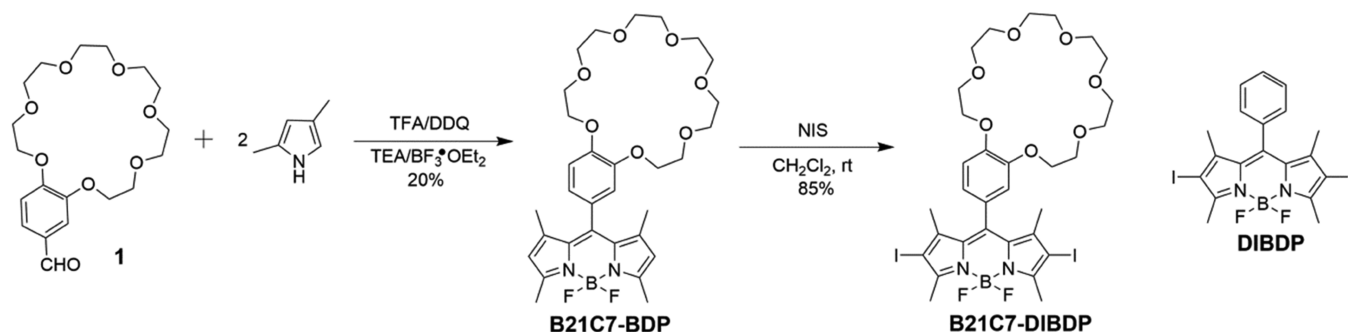
[a]The molecular structure of the reference compound **DIBDP** is also shown in this scheme.

Figure 1. Selected frontier molecular orbitals of **B21C7-DIBDP**. The calculations are based on the optimized ground-state geometry (S_0 state) without any solvent at the B3LYP/6-31G(d) level using Gaussian 09W.

Crown ethers have been widely exploited and applied in numerous areas, such as supramolecular polymers,[53−57] fluorescence probes and sensors,[58−61] molecular machines,[62−67] and ionic channels,[68] since the 1987 Nobel Prize for Chemistry was awarded to Pedersen,[69] Cram,[70] and Lehn.[71] Among them, fluorophore-functionalized crown ethers utilized in constructing supramolecular fluorescence systems that were usually based on photoinduced electron-transfer (PET) mechanisms between the hosts and guests were widely applied in fluorescence probes and sensors;[58−61] however, fabricating triplet-photosensitizer-functionalized crown ether systems remains an enormous challenge due to very few investigations on them.[72] Previously, we prepared a **DIBDP**-functionalized ethoxypillar[5]arene (**EtP5**) and confirmed that the steric hindrance of **EtP5** could reduce collision and further weaken the TTA self-quenching effects of **DIBDP** moieties.[51] However, to the best of our knowledge, the electron-transfer mechanism in triplet-photosensitizer-functionalized crown

ethers has not been investigated so far, and the influences of electron-rich cavities of crown ethers on the triplet-state lifetimes of photosensitizers in photosensitizer-functionalized crown ether are still not clear. All of these are major obstacles and challenges to designing and assembling supramolecular smart nanostructures, including excellent PDT materials, photocatalysis, and photovoltaic devices based on photosensitizer-functionalized crown ethers.

Herein, we designed and synthesized a benzo-21-crown-7 (**B21C7**)-functionalized **DIBDP** (**B21C7-DIBDP**) (Scheme 1). Systematic investigations of calculations of density functional theory (DFT), photophysical properties, electrochemical properties, and nanosecond time-resolved transient absorption spectra were performed to work out the electron-transfer mechanisms between crown ethers and **DIBDP** moieties, as well as the strategies of weakening the TTA self-quenching effect of **DIBDP** moieties.

2. RESULTS AND DISCUSSION

2.1. Design and Synthesis of the Target Molecule. As stated in Section 1, the TTA self-quenching effect induced by sensitizers,[47,49−51] and how to weaken the TTA self-quenching effect of triplet sensitizers is a critical issue that needs to be resolved. Inspired by our previous work, owing to the huge bulks, pillar[5]arenes connected by methylene bridges at the para-positions of five 2,5-dialkoxybenzene rings could weaken the TTA self-quenching effect induced by the photosensitizers.[51] Herein, we attempted to introduce another supramolecular macrocycle (**B21C7**) connected by seven ethylene glycol units that contain electron-rich cavities and huge bulks as well.[57] Moreover, due to the excellent photophysical properties of **DIBDP**,[42,47,48,50−52] as well as both **DIBDP** and **B21C7** being readily functionalized,[42,47,48,50−52,57] **B21C7**-substituted **BODIPY** (**B21C7-BDP**) was prepared according to a literature report,[73] followed by the iodization of **B21C7-BDP** to obtain **B21C7-DIBDP**. Both **B21C7-BDP** and **B21C7-DIBDP** could be prepared in satisfactory yields (Scheme 1). The molecular structure of **B21C7-DIBDP** was systematically verified by melt points, ^{1}H nuclear magnetic resonance (NMR), ^{13}C NMR, and high-resolution mass spectra (HRMS) (Figures S1−S3). Furthermore, similar to **DIBDP**-functionalized pillar[5]arene in our previous work,[51] the electron-transfer effect of electron-rich **B21C7** moieties on both singlet and triplet states of **DIBDP** moieties was also expected to be systematically investigated in **B21C7**-functionalized **DIBDP**.

2.2. DFT/TDDFT Computations. DFT calculations using Gaussian 09W were effective auxiliary tools for predicting the electron-transfer process from the **B21C7** moiety to the **DIBDP** moiety in **B21C7-DIBDP** prior to the experimental investigations.[51] From the highest occupied molecular orbital (HOMO)−lowest unoccupied molecular orbital (LUMO) distributions of the low-lying singlet state (S$_1$) of **B21C7-DIBDP** (Figure 1), no overlaps were observed between the initial and the destination molecular orbital (MO) involved in the transitions of **B21C7-DIBDP**, which indicates that the forbidden S$_0$ → S$_1$ transition and the emission intensity of **B21C7-DIBDP** may be weaker than **DIBDP**. It could be speculated from the DFT/TDDFT calculated results that there may be an electron-transfer process from the **B21C7** moiety to the **DIBDP** moiety in **B21C7-DIBDP**.

The isosurfaces of spin densities of **DIBDP** and **B21C7-DIBDP** were exported from their optimized lowest-lying triplet-state (T$_1$) geometries based on their optimized geometries of the S$_0$ state, respectively (Figure 2), at the DFT//B3LYP/6-31G(d) level using Gaussian 09W.[74−76] However, unlike the HOMO−LUMO distributions of the S$_1$ state of **B21C7-DIBDP**, the isosurface of the spin density of **B21C7-DIBDP** was not localized on the **B21C7** moiety but on the **DIBDP** moiety, which indicated that the electron-rich cavity of **B21C7** had no direct effect on the T$_1$ state of the **DIBDP** moiety. As seen from Figures 1 and 2, the possible existing electron-transfer process in **B21C7-DIBDP** from the **B21C7** moiety to the **DIBDP** moiety could only affect the S$_0$ → S$_1$ transition of the **DIBDP** moiety but not the ISC of S$_1$ states. Next, these computational results will be further verified using experimental strategies.

2.3. Spectroscopic and Photophysical Properties. The basic spectroscopic (Figures 3 and 5) and photophysical
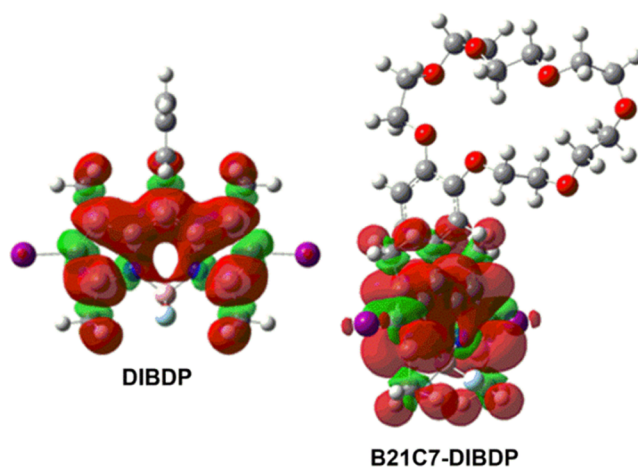
Figure 2. Isosurfaces of the spin densities of **DIBDP** and **B21C7-DIBDP** based on the optimized triplet-state geometries. The calculations were performed at the B3LYP/6-31G(d) level using Gaussian 09W.
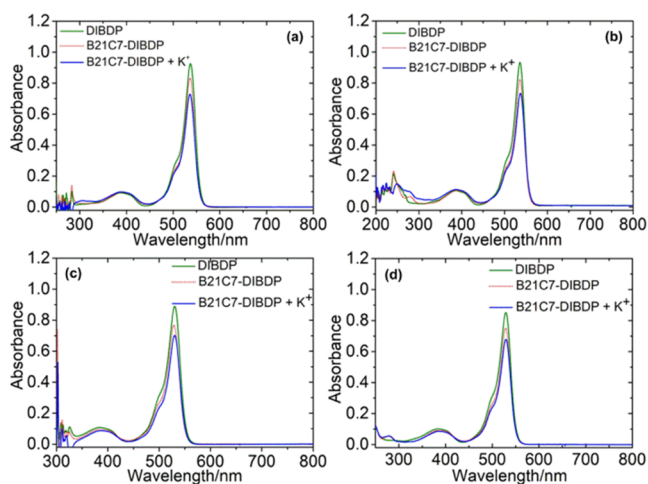
Figure 3. UV−vis absorption spectra of **DIBDP** and **B21C7-DIBDP** (1.0×10^{-5} M, 25 °C) in toluene (a), CHCl$_3$ (b), acetone (c), and CH$_3$CN (d).

properties (Table 1) were investigated first. In comparison to the characteristic absorptions of **DIBDP** in Figure 3, the strong absorption bands of **B21C7-DIBDP** at ∼530 nm in toluene, CHCl$_3$, acetone, and CH$_3$CN are all absorptions of **DIBDP** chromophores in **B21C7-DIBDP** (Figure 3). Both maximum absorption wavelengths of **DIBDP** and **B21C7-DIBDP** exhibited a hypsochromic shift to shorter wavelengths, and the decreasing intensities at maximum absorption wavelengths with the polarity of solvents increasing (Table 1) indicated that there were also n−π transitions besides π−π transitions in these two molecules because both contained nonbonding electrons in the atoms of nitrogen, iodine, and fluorine. However, the absorption intensities of **B21C7-DIBDP** at maximum absorption wavelengths were weaker than those of **DIBDP** in the same solvent (Figure 3 and Table 1), which could be attributed to the electron transfer from **B21C7** moieties to **DIBDP** moieties. Furthermore, the maximum absorption intensities of **B21C7-DIBDP** became weaker when 1.0 equiv of KPF$_6$ was added in the above-mentioned four solvents (Figure 3 and Table 1). Thus, it could be seen that the hyperchromic effect of electron-rich **B21C7** on the **DIBDP**

Table 1. Photophysical Parameters of DIBDP and B21C7-DIBDP in Toluene (TOL), CHCl$_3$ (CHL), Acetone (ACE), and CH$_3$CN (ACN)

solvent	compd	λ_{abs} (nm)[a]	ε[b]	λ_{em} (nm)[c]	Φ_F (%)[d]	τ_F (ns)[e]	τ_{T1} (μs)[f]	τ_T (μs)[g]
TOL	**DIBDP**	537	0.87	556	1.9[i]	0.27	45	126
	B21C7-DIBDP	536	0.83	553	1.7	0.28	**59**	125
	B21C7-DIBDP⊃K$^+$[h]	536	0.73	554	1.3	0.18	60	136
CHL	**DIBDP**	536	0.88	553	2.0[i]	0.29	66	142
	B21C7-DIBDP	536	0.81	552	1.7	0.32	**99**	145
	B21C7-DIBDP⊃K$^+$[h]	537	0.72	555	1.4	0.16	104	144
ACE	**DIBDP**	531	0.83	550	1.5[i]	0.12	43	130
	B21C7-DIBDP	529	0.78	548	1.1	0.07	**66**	136
	B21C7-DIBDP⊃K$^+$[h]	530	0.72	548	1.3	0.15	63	139
ACN	**DIBDP**	529	0.81	550	1.5[i]	0.17	41	114
	B21C7-DIBDP	529	0.76	548	0.8	0.04	**78**	117
	B21C7-DIBDP⊃K$^+$[h]	529	0.69	548	1.1	0.10	75	118

[a]Maximum absorption wavelength ($c = 1.0 \times 10^{-5}$ M). [b]Molar extinction coefficient, in 10^5 M^{-1} cm^{-1}. [c]Maximum emission wavelength ($c = 1.0 \times 10^{-5}$ M). [d]Absolute fluorescence quantum yields. [e]Fluorescence lifetimes. [f]Triplet-state lifetimes ($c = 1.0 \times 10^{-5}$ M). [g]Intrinsic triplet-state lifetimes obtained by fitting experimental curves using a kinetic model supposing the TTA self-quenching effect eliminated.[77] [h]Molar ratio of 1:1. [i]Literature-reported value.

moiety became weaker after the K$^+$ entered the B21C7's cavity because a proportion of electrons of **B21C7** was transferred to K$^+$, as well as the increase in the solvents' polarities after adding KPF$_6$ could have weakened the maximum absorption intensities of **B21C7-DIBDP** due to the n−π transitions in **B21C7-DIBDP**. The UV−vis absorption spectra in Figure 3 preliminarily verified that there were electron-transfer processes from the **B21C7** moiety to the **DIBDP** moiety in **B21C7-DIBDP** in toluene, CHCl$_3$, acetone, and CH$_3$CN.

The PET processes, which included a-PET (the photo-induced electron-transfer process from the electron donor to the fluorophore that is an electron acceptor) and d-PET processes (the photoinduced electron-transfer process from the fluorophore (donor) to the electron acceptor), are illustrated in Figure 4. We have verified the a-PET (Figure
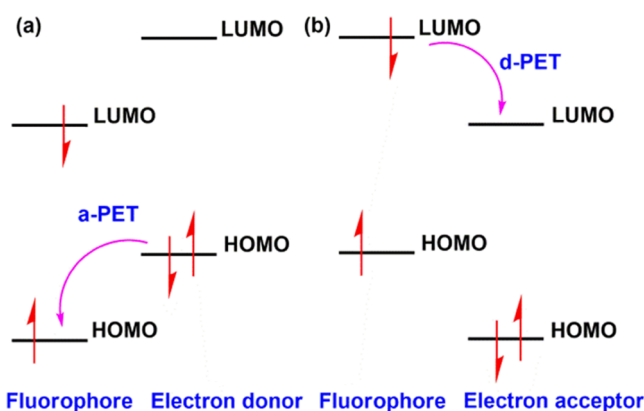
Figure 4. Frontier molecular orbitals of fluorescecet molecules with PET processes. (a) a-PET process: photoinduced electron-transfer process from the electron donor to the fluorophore, which is an electron acceptor; (b) d-PET process: photoinduced electron-transfer process from the fluorophore (donor) to the electron acceptor.

4a) effect between **EtP5** and **DIBDP** moieties in **DIBDP**-functionalized pillar[5]arene in our previous work.[51] To investigate the electron-transfer process between **B21C7** and **DIBDP** moieties in **B21C7-DIBDP**, the fluorescence emissions of **DIBDP**, **B21C7-DIBDP**, and **B21C7-DIBDP⊃K$^+$** were investigated in a variety of solvents with

different polarities (Figures 5 and S4−S9). First, the emission intensities of **B21C7-DIBDP** were slightly weaker than those
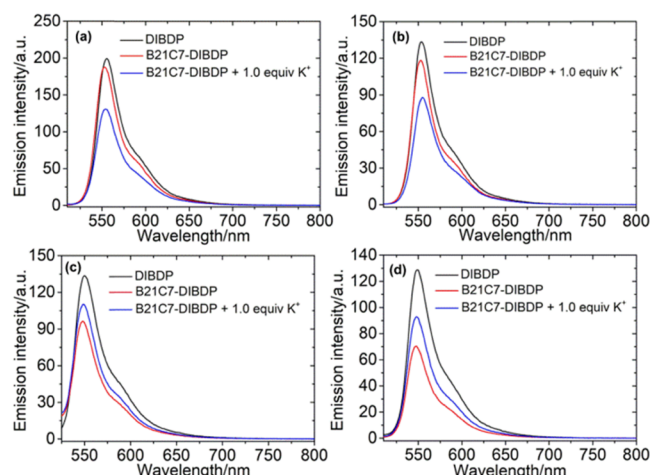

Figure 5. Fluorescence emission spectra of **DIBDP** and **B21C7-DIBDP** (1.0×10^{-5} M, 25 °C) in toluene (a), CHCl$_3$ (b), acetone (c), and CH$_3$CN (d).

of **DIBDP** in toluene and CHCl$_3$; however, the emission intensities of **B21C7-DIBDP** were quenched more seriously when K$^+$ was added (Figure 5a,b), which indicated that there were more obvious electron-transfer processes when the polarities of the solvents became higher after K$^+$ was added. Second, interestingly, the opposite experimental results were obtained in acetone and CH$_3$CN (Figure 5c,d). The emission intensities of **B21C7-DIBDP** were quenched more seriously in acetone and CH$_3$CN than those in toluene and CHCl$_3$, which verified again that the electron-transfer processes could easily occur in higher polar solvents. When K$^+$ was added, the emission intensities of **B21C7-DIBDP** were boosted in acetone and CH$_3$CN because the complexations of **B21C7** moiety with K$^+$ made the electron-transfer effects from the **B21C7** moiety to the **DIBDP** moiety weaker. Upon investigating the fluorescence emission experiments of **DIBDP**, **B21C7-DIBDP**, and **B21C7-DIBDP⊃K$^+$** in a variety of solvents with different polarities, the electron-transfer effect between **B21C7** and **DIBDP** moieties in **B21C7-DIBDP** (a-

PET) was further confirmed. In addition, the other photophysical properties of **DIBDP** and **B21C7-DIBDP** are listed in Table 1. According to the a-PET process in Figure 4a, the electron transfer from the **B21C7** moiety to the **DIBDP** moiety resulted in the HOMO orbitals of **DIBDP** moieties being occupied by the electrons of **B21C7** moieties, and a proportion of the produced singlet states of **DIBDP** moieties could not emit fluorescence in the form of radiation transition. Therefore, the fluorescence quantum yields of **B21C7-DIBDP** were smaller than those of **DIBDP** in the same solvents (Table 1).

2.4. Electrochemical Investigations. To verify the a-PET process from the **B21C7** moiety to the **DIBDP** moiety in **B21C7-DIBDP** qualitatively and quantitatively, the electrochemical properties of **B21C7-DIBDP** and reference compounds **DIBDP** and **B21C7** were investigated using cyclic voltammetry (Figure 6). **B21C7** showed a reversible oxidation
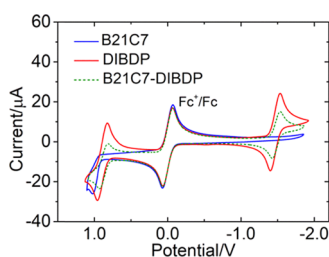
Figure 6. Cyclic voltammograms of **B21C7**, **DIBDP**, and **B21C7-DIBDP** in deaerated CH_2Cl_2 containing 1.0 mM compound to be measured and ferrocene (Fc), 0.10 M Bu_4NPF_6 as the supporting electrolyte, and $Ag/AgNO_3$ as the reference electrode; scan rate was 0.1 V/s, 25 °C. Fc was used as the internal reference [$E_{1/2}$ = +0.64 V (Fc^+/Fc) vs the standard hydrogen electrode].

potential at +0.98 V (vs Fc/Fc^+), and no reduction potential was observed from 0 to −2.0 V, indicating that the **B21C7** moiety was suitable for being an electron donor (Figure 6 and Tables 2 and 3).[51] However, interestingly, after the **B21C7** moiety modified to **DIBDP**, the oxidation potential of **B21C7-DIBDP** was at +0.87 V (vs Fc/Fc^+) and the initial oxidation potential of **B21C7** at +0.98 V disappeared due to the electron transfer from the **B21C7** moiety to the **DIBDP** moiety. Moreover, both oxidation and reduction potentials of **B21C7-DIBDP** were similar to those of **DIBDP** (Figure 6 and Tables 2 and 3). Cyclic voltammograms in Figure 6 qualitatively demonstrate the existence of the electron-transfer process from the **B21C7** moiety to the **DIBDP** moiety in **B21C7-DIBDP**.

To clarify the direction and limitation of the influences of electron-transfer processes in **B21C7-DIBDP** on the fluorescence emission and the T_1 state of the **DIBDP** moiety

quantitatively, Gibbs free energy changes (ΔG_{CS}) of the electron transfer as well as the energy levels of charge separation states (E_{CS}) of **B21C7-DIBDP** were determined using Weller equations (eqs 1−3).[78]

$$\Delta G_S = -\frac{e^2}{4\pi\varepsilon_S\varepsilon_0 R_{CC}} - \frac{e^2}{8\pi\varepsilon_0}\left(\frac{1}{R_D} + \frac{1}{R_A}\right)\left(\frac{1}{\varepsilon_{REF}} - \frac{1}{\varepsilon_S}\right) \tag{1}$$

$$\Delta G_{CS} = e[E_{OX} - E_{RED}] - E_{00} + \Delta G_S \tag{2}$$

$$E_{CS} = e[E_{OX} - E_{RED}] + \Delta G_S \tag{3}$$

where ΔG_S is the static Coulombic energy, which was determined by eq 1. e is the elementary charge, E_{OX} is the half-wave potential for one electron oxidation in the electron-donor unit, E_{RED} is the half-wave potential for one electron reduction of the electron-acceptor unit, and E_{00} is the energy level calculated with the fluorescence emission wavelength (S_1) or the phosphorescent emission wavelength (T_1). ε_S is the static dielectric constant of the solvent. R_{CC} is the center-to-center separation distance between the electron donor and the electron acceptor, determined by the optimized geometry of DFT calculations. R_D is the radius of the electron donor; R_A is the radius of the electron acceptor. ε_{REF} is the static dielectric constant of the solvent used for the electrochemical studies. ε_0 is the permittivity of free space. ΔG_{CS} is the Gibbs free energy changes, which was determined by eq 2. E_{CS} is energy of the charge-separated states, which was determined by eq 3. The calculated results of ΔG_{CS} and E_{CS} for the influence on fluorescence emission (E_{00} is the energy level approximated with the fluorescence emission wavelength) of the **DIBDP** moiety in **B21C7-DIBDP** are listed in Table 2; however, the results for the influence on the T_1-state lifetime (E_{00} is the energy level approximated with phosphorescent emission wavelength) of the **DIBDP** moiety in **B21C7-DIBDP** are listed in Table 3.

When E_{00} was the energy level of the fluorescence emission (S_1), the ΔG_{CS} values were 0.01, −0.10, −0.19, and −0.21 eV for the electron-transfer processes from the **B21C7** moiety to the **DIBDP** moiety in toluene, $CHCl_3$, acetone, and CH_3CN, respectively (Table 2). The corresponding E_{CS} values in $CHCl_3$, acetone, and CH_3CN were 2.14, 2.06, and 2.05, respectively (Table 2), and were all lower than the corresponding S_1-state energies of **DIBDP** moieties (2.25 eV). However, in toluene, the ΔG_{CS} value for the electron-transfer process in **B21C7-DIBDP** was greater than 0 and the E_{CS} value of **B21C7-DIBDP** was higher than the S_1-state energy of **DIBDP** moieties (2.25 eV). These calculation results demonstrated that the electron-transfer processes from **B21C7** moieties to **DIBDP** moieties influenced the fluorescence

Table 2. Electrochemical Redox Potentials[a], Gibbs Free Energy Changes (ΔG_{CS}), and Charge Separation Energy States (E_{CS})[b] for B21C7, DIBDP, and B21C7-DIBDP in Toluene (TOL), CHCl₃ (CHL), Acetone (ACE), and CH₃CN (ACN)

compd	E_{OX} (V)	E_{RED} (V)	ΔG_{CS} (eV)				E_{CS} (eV)			
			TOL	CHL	ACE	ACN	TOL	CHL	ACE	ACN
B21C7	+0.98	c	d	d	d	d	d	d	d	d
DIBDP	+0.89	−1.47	d	d	d	d	d	d	d	d
B21C7-DIBDP	+0.87	−1.48	0.01	−0.10	−0.19	−0.21	2.25	2.14	2.06	2.05

[a]The values of redox potentials were obtained by setting the potential of Fc^+/Fc as 0 V, measured in deaerated CH_2Cl_2. The counter electrode was a Pt electrode, and the working electrode was a glassy carbon electrode, with a $Ag/AgNO_3$ couple as the reference electrode. [b]E_{00} is the energy level of the fluorescence emission. [c]Not been observed. [d]Unable to be determined.

Table 3. Electrochemical Redox Potentials[a], Gibbs Free Energy Changes (ΔG_{CS}), and Charge Separation Energy States (E_{CS})[b] for B21C7, DIBDP, and B21C7-DIBDP in Toluene (TOL), CHCl₃ (CHL), Acetone (ACE), and CH₃CN (ACN)

compd	E_{OX} (V)	E_{RED} (V)	ΔG_{CS} (eV)				E_{CS} (eV)			
			TOL	CHL	ACE	ACN	TOL	CHL	ACE	ACN
EtP5	+0.98	c	d	d	d	d	d	d	d	d
DIBDP	+0.89	−1.47	d	d	d	d	d	d	d	d
EtP5-DIBDP	+0.87	−1.48	0.59	0.49	0.41	0.38	2.25	2.14	2.06	2.05

[a]The values of redox potentials were obtained by setting the potential of Fc⁺/Fc as 0 V, measured in deaerated CH₂Cl₂. The counter electrode was a Pt electrode, and the working electrode was a glassy carbon electrode, with a Ag/AgNO₃ couple as the reference electrode. [b]E_{00} is the energy level of the T₁ state. [c]Not been observed. [d]Unable to be determined.

emission of **DIBDP** moieties in CHCl₃, acetone, and CH₃CN except for that in toluene. Simultaneously, the fluorescence emissions of **DIBDP** moieties were easier to be affected by the electron-transfer processes in higher polar solvents, which were in agreement with the fluorescence emission spectra in Figure 5.

When E_{00} was the energy level of the T₁ state of **DIBDP** (1.61 eV), the ΔG_{CS} values were 0.59, 0.49, 0.41, and 0.38 eV for the electron-transfer processes from the **B21C7** moiety to the **DIBDP** moiety in toluene, CHCl₃, acetone, and CH₃CN, respectively (Table 3). The ΔG_{CS} values in these four solvents were all greater than 0, and the corresponding E_{CS} values were all higher than the T₁-state energy of **DIBDP** moieties (Table 3). These calculated results demonstrated that the electron-transfer processes from **B21C7** moieties to **DIBDP** moieties in **B21C7-DIBDP** could not directly affect the T₁ states of **DIBDP** moieties in all of the above four solvents due to the exceedingly low T₁ energy state of **DIBDP** (1.61 eV).

2.5. Nanosecond Time-Resolved Transient Absorption Spectroscopy. DFT calculations and electrochemical investigations demonstrated that there were no direct influences on the electron-transfer process on the T₁ states of **DIBDP** moieties in **B21C7-DIBDP**. Herein, nanosecond time-resolved transient absorption spectra were used to verify the results of DFT calculations and electrochemical investigations further (Figures S26−S34). Simultaneously, we fitted the intrinsic triplet-state lifetimes of **DIBDP** and **B21C7-DIBDP** in these four solvents according to eqs 4−6.[47,50,77] The differential equation in the decaying process of the triplet state is expressed in eq 4.

$$\frac{dc_T}{dt} = -k_1 c_T - k_2 c_T^2 \tag{4}$$

where c_T is the concentration of the triplet state, t is the decaying time, k_1 is the spontaneous decaying rate constant without the TTA self-quenching effect, and k_2 is the bimolecular decaying rate constant induced by the TTA self-quenching effect. Moreover, the corresponding integral equation is expressed in eq 5.

$$c_T(t) = \frac{c_0 k_1}{\exp(k_1 t) \cdot (c_0 k_2 + k_1) - c_0 k_2} \tag{5}$$

where c_0 is the initial concentration of triplet states and $c_T(t)$ is the concentration of triplet states at time t. The transient absorption intensity at time t is expressed in eq 6.

$$A(t) = \frac{A_0 \tau_2 / \tau_1}{\exp(t/\tau_1) \cdot (1 + \tau_2/\tau_1) - 1} \tag{6}$$

where $A(t)$ is the transient absorption intensity at time t. A_0 is the initial transient absorption intensity prior to decaying. τ_1 is

the unimolecular lifetime of the triplet state without the TTA self-quenching effect induced by the photosensitizers. $\tau_2 = 1/c_0 k_2$, which is the reciprocal of the initial concentration of the triplet state multiply the bimolecular decaying rate constant induced by the TTA self-quenching effect of the photosensitizers. The triplet-state lifetime values of the photosensitizers were fitted using eq 6 with three variables (A_0, τ_1, τ_2) supposing that the TTA self-quenching effect was eliminated.[47,50,77]

First, the maps of transient absorption for **DIBDP** and **B21C7-DIBDP** in various solvents were very similar (Figures S26−S33), verifying that **B21C7** moieties could not affect the T₁ states of **DIBDP** moieties in **B21C7-DIBDP**. Second, the lifetimes of **B21C7-DIBDP** in toluene, CHCl₃, acetone, and CH₃CN were obviously longer than those of **DIBDP** at a high concentration (1.0 × 10⁻⁵ M); moreover, the lifetimes of **B21C7-DIBDP** in these four solvents almost remained unchanged when K⁺ was added (Figure S34). Third, the intrinsic triplet-state lifetimes values of **B21C7-DIBDP** were slightly greater than **DIBDP** in the same solvents, for instance, in Figure S34b,f,j. The above experimental results demonstrated that there were no direct effects of the electron transfer from the **B21C7** moiety to the **DIBDP** moiety in **B21C7-DIBDP** on the intrinsic triplet-state lifetimes. Moreover, the huge bulks of **B21C7** moieties resulting in steric hindrance (Figure 7) could reduce the collision of **DIBDP** moieties and
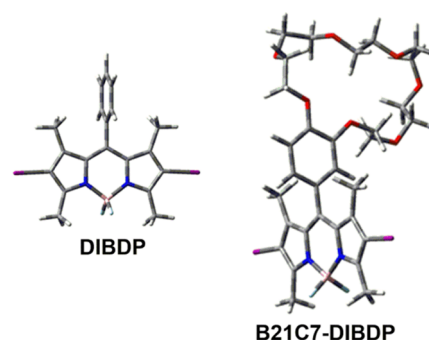
Figure 7. Optimized ground-state geometries of **DIBDP** and **B21C7-DIBDP** at the DFT//B3LYP/6-31G(d) level using Gaussian 09W.

further weaken the TTA self-quenching effect (the TTA process needs collision of sensitizers in the range of 0−1 nm[31,35,36]) of **DIBDP** moieties in **B21C7-DIBDP** at a high concentration (1.0 × 10⁻⁵ M). The fluorescence quantum yields of **B21C7-DIBDP** were observed to be greater in nonpolar solvents compared to those in polar solvents; this was because the stronger a-PET effects induced smaller fluorescence quantum yields in polar solvents, while the TTA self-quenching effects were weakened more efficiently in polar

solvents (Table 1). As illustrated in Figure 4a, when the outer-layer valence electron of **DIBDP** moieties in **B21C7-DIBDP** was transited from the HOMO orbital to the LUMO orbital, as a result of the a-PET effect, the HOMO orbitals of **DIBDP** moieties were occupied by the electrons in **B21C7** moieties so that singlet states of **DIBDP** moieties could not emit fluorescence in the form of radiation transition but could be transformed to triplet states through the ISC process due to the iodine atoms in the **DIBDP** moiety. Therefore, the stronger a-PET effects in polar solvents induced smaller fluorescence quantum yields but weaker TTA self-quenching effects (Table 1).

3. CONCLUSIONS

In summary, we designed and synthesized a **B21C7**-functionalized **DIBDP** (**B21C7-DIBDP**) to investigate the influences of huge bulks and electron-rich cavities of **B21C7** moieties on the fluorescence emission and triplet-state lifetimes of **DIBDP** moieties. DFT/TDDFT computable results preliminarily predicted that **B21C7** moieties had direct influences on the fluorescence emissions of **DIBDP** moieties but not on their localization of triplet states of **B21C7-DIBDP**. The UV−vis absorption spectra, fluorescence emission spectra, and cyclic voltammograms verified that there was an electron-transfer process from the **B21C7** moiety to the **DIBDP** moiety (a-PET) in **B21C7-DIBDP**. However, the calculated results of ΔG_{CS} and E_{CS} values, nanosecond time-resolved transient absorption spectra, and intrinsic triplet-state lifetimes demonstrated that the electron-transfer processes from the **B21C7** moiety to the **DIBDP** moiety in **B21C7-DIBDP** had direct influences on the fluorescence emission of **DIBDP** moieties but not on the triplet states of **DIBDP** moieties. The triplet-state lifetimes of **B21C7-DIBDP** were obviously longer than **DIBDP** at a high concentration (1.0×10^{-5} M); however, the fitted values of intrinsic triplet-state lifetimes of **B21C7-DIBDP** were only slightly greater than those of **DIBDP** in the same solvent. Besides the steric hindrance of **B21C7** moieties, which could weaken the TTA self-quenching effect of **DIBDP** moieties at a high concentration, the a-PET effect resulted in a proportion of the produced singlet states of **DIBDP** moieties not being able to emit fluorescence in the form of radiation transition, but they could be transformed to triplet states through ISC processes due to the iodine atoms in the **DIBDP** moiety. The stronger a-PET effects in polar solvents induced smaller fluorescence quantum yields so that more singlet states of **DIBDP** moieties were transformed to triplet states to weaken the TTA self-quenching effects. These experimental results provided another strategy of weakening the TTA self-quenching effect induced by the sensitizers; thus, they will be significant for designing and assembling supramolecular smart nanostructures, including excellent PDT materials, photocatalysis, and photovoltaic devices based on photosensitizer-functionalized crown ethers.

4. METHODS

4.1. Synthesis and Characterizations. All of the raw materials were analytically pure and used without further purification. The organic solvents were dried or distilled before use. Thin-layer chromatography (TLC) and column chromatography were carried out using silica gel (200−300 mesh) as the stationary phase. Melting points were measured on an SHPSIC WRS-2 automatic melting point apparatus (China).

^{1}H NMR and ^{13}C NMR spectra were obtained on a Bruker AVANCE 400 spectrophotometer (Germany) with CDCl$_3$ as the solvent and Si(CH$_3$)$_4$ as the internal standard (0.00 ppm). High-resolution mass spectra (HRMS) were recorded in an ion trap ESI-HRMS spectrometer. Detailed synthetic routes for **B21C7-DIBDP** are shown in Scheme 1; please see the Supporting Information for the structural characterizations.

4.2. Instruments for Spectral Measurement. The UV−vis absorption spectra were recorded on an HP8453 UV−vis spectrophotometer. The fluorescence emission spectra were measured with an FS5 spectrofluorometer (Edinburgh Instrument Ltd., U.K.). The absolute fluorescence quantum yields were determined by a C13534 UV−NIR spectrometer, equipped with an optical integration sphere (Hamamatsu Photonics K.K., Japan). Fluorescence lifetimes were recorded on an OB920 luminescent lifetime spectrometer (Edinburgh Instruments Ltd., U.K.) equipped with a 510 nm EPL picosecond pulsed laser for excitation, and the decay traces were measured with the time-correlated single photon counting (TCSPC) technique. Cyclic voltammograms were performed using a CHI610D electrochemical workstation (Shanghai, China). The nanosecond time-resolved transient absorption spectra were measured with an LP980 laser flash photolysis spectrometer (Edinburgh Instruments Ltd., U.K.). Opolette HE 355 UV tunable laser systems (OPOTEK Inc.) were used for excitation (210−2400 nm). Typical laser power was 5 mJ per pulse. The signal was digitized on a Tektronix TDS 3012B oscilloscope.

4.3. Details of Theoretical Computations. The ground-state (S$_0$) geometries of **DIBDP** and **B21C7-DIBDP** were optimized based on DFT with the B3LYP functional[74] and the 6-31G(d) basis set.[75] The isosurfaces of spin density and excited-state energies of **DIBDP** and **B21C7-DIBDP** were calculated using DFT and time-dependent DFT (TDDFT), respectively, based on the optimized geometries of the S$_0$ state. All of these calculations were performed using the Gaussian 09W program package suite in a Dell server.[76]

4.4. Methods of Electrochemical Studies. Cyclic voltammogram curves were recorded at a scan rate of 0.1 V/s. The electrolytic cell was a three-electrode-containing cell. Electrochemical measurements were performed in CH$_2$Cl$_2$ with ferrocene (Fc) as the internal reference and 0.1 M Bu$_4$NPF$_6$ as the supporting electrolyte after deaerated by high-purity N$_2$. The working electrode was a glassy carbon electrode, and the counter electrode was a platinum electrode. In addition, a nonaqueous Ag/AgNO$_3$ (0.1 M in CH$_3$CN) reference electrode was contained in a separate compartment connected to the solution via a semipermeable membrane.[78]

4.5. Measuring Method for Nanosecond Time-Resolved Transient Absorption Spectroscopy. All of the samples of **DIBDP** and **B21C7-DIBDP** were deaerated by high-purity N$_2$ for 15 min and well-sealed by a parafilm prior to measurement. The fitted values of triplet-state lifetimes and the maps of transient absorption of the samples were obtained in L900 software. The intrinsic triplet-state lifetimes were obtained by fitting experimental curves using a kinetic model, supposing that the TTA self-quenching effect was eliminated.[77]

4.6. Synthetic Procedures of B21C7-DIBDP. Compounds **1** and **B21C7-BDP** were prepared according to a literature report,[73] and the synthetic procedures of **B21C7-DIBDP** have been described as follows.

B21C7-BDP (1.2 g, 2.0 mmol) was dissolved in anhydrous CH$_2$Cl$_2$ (250 mL), and then excess *N*-iodosuccinimide (1.8 g, 8.0 mmol) was added. The mixture was stirred at room temperature overnight. The reaction mixture was then washed using brine three times and concentrated under a vacuum. The crude product was purified by flash column chromatography (CH$_2$Cl$_2$/EtOAc, 5:1, v/v). The red band was collected, and the solvent was removed under reduced pressure to give the product as a red solid. Yield: 1.5 g, 85.0%. MP: 168.8−169.5 °C. The ^{1}H NMR spectrum of **B21C7-DIBDP** is shown in Figure S1. ^{1}H NMR (400 MHz, CDCl$_3$): δ 6.99−6.97 (d, 1H, *J* = 8.0 Hz), 6.78−6.74 (m, 2H), 4.24−4.22 (t, 2H, *J* = 4.0 Hz), 4.12−4.10 (t, 2H, *J* = 4.0 Hz), 3.99−3.97 (t, 2H, *J* = 4.0 Hz), 3.93−3.91 (t, 2H, *J* = 4.0 Hz), 3.86−3.84 (t, 2H, *J* = 4.0 Hz), 3.81−3.75 (m, 6H), 3.70 (s, 8H), 2.64 (s, 6H), 1.48 (s, 6H). The ^{13}C NMR spectrum of **B21C7-DIBDP** is shown in Figure S2. ^{13}C NMR (100 MHz, CDCl$_3$): δ 156.6, 149.8, 144.8, 141.2, 132.9, 131.6, 129.8, 128.0, 127.1, 120.8, 114.0, 113.3, 85.6, 70.5, 68.6, 63.6, 31.9, 29.6, 21.6, 17.1, 16.0. The ESI-HRMS spectrum of **B21C7-DIBDP** is shown in Figure S3. ESI-HRMS: calcd [C$_{31}$H$_{39}$BF$_2$I$_2$N$_2$O$_7$ + NH$_4^+$] *m/z* = 872.1246, found *m/z* = 872.1253, error: 0.0007; calcd [C$_{31}$H$_{39}$BF$_2$I$_2$N$_2$O$_7$ + Na$^+$] *m/z* = 877.0800, found *m/z* = 877.0805, error: 0.0005.

ASSOCIATED CONTENT

ⓈⒾ Supporting Information

The Supporting Information is available free of charge at https://pubs.acs.org/doi/10.1021/acsomega.1c04540.

Characterization data, spectroscopic data, and DFT/TDDFT calculation details (PDF)

AUTHOR INFORMATION

Corresponding Authors

Jifu Sun − *College of Chemical and Biological Engineering, Shandong University of Science and Technology, Qingdao 266590, P. R. China;* ⓞ orcid.org/0000-0001-7536-9759; Email: sunjifu2019@sdust.edu.cn

Bo Wang − *College of Chemical and Biological Engineering, Shandong University of Science and Technology, Qingdao 266590, P. R. China;* ⓞ orcid.org/0000-0003-4226-4963; Email: wb@sdust.edu.cn

Jianzhang Zhao − *State Key Laboratory of Fine Chemicals, Dalian University of Technology, Dalian 116024, P. R. China;* ⓞ orcid.org/0000-0002-5405-6398; Email: zhaojzh@dlut.edu.cn

Authors

Weixu Li − *College of Chemical and Biological Engineering, Shandong University of Science and Technology, Qingdao 266590, P. R. China*

Yuqi Hou − *State Key Laboratory of Fine Chemicals, Dalian University of Technology, Dalian 116024, P. R. China;* ⓞ orcid.org/0000-0002-8175-6568

Xue Zhang − *State Key Laboratory of Fine Chemicals, Dalian University of Technology, Dalian 116024, P. R. China;* ⓞ orcid.org/0000-0003-3681-202X

Zhongzheng Gao − *College of Chemical and Biological Engineering, Shandong University of Science and Technology, Qingdao 266590, P. R. China*

Complete contact information is available at:
https://pubs.acs.org/10.1021/acsomega.1c04540

Notes

The authors declare no competing financial interest.

ACKNOWLEDGMENTS

REFERENCES

(1) Chen, K. K.; Guo, S.; Liu, H.; Li, X.; Zhang, Z. M.; Lu, T. B. Strong Visible-Light-Absorbing Cuprous Sensitizers for Dramatically Boosting Photocatalysis. *Angew. Chem., Int. Ed.* **2020**, *59*, 12951−12957.

(2) Hari, D. P.; Konig, B. The Photocatalyzed Meerwein Arylation: Classic Reaction of Aryl Diazonium Salts in a New Light. *Angew. Chem., Int. Ed.* **2013**, *52*, 4734−4743.

(3) Linic, S.; Christopher, P.; Ingram, D. B. Plasmonic-Metal Nanostructures for Efficient Conversion of Solar to Chemical Energy. *Nat. Mater.* **2011**, *10*, 911−921.

(4) Prier, C. K.; Rankic, D. A.; MacMillan, D. W. Visible Light Photoredox Catalysis with Transition Metal Complexes: Applications in Organic Synthesis. *Chem. Rev.* **2013**, *113*, 5322−5363.

(5) Tian, J.; Xu, Z. Y.; Zhang, D. W.; Wang, H.; Xie, S. H.; Xu, D. W.; Ren, Y. H.; Wang, H.; Liu, Y.; Li, Z. T. Supramolecular Metal-Organic Frameworks That Display High Homogeneous and Heterogeneous Photocatalytic Activity for H$_2$ Production. *Nat. Commun.* **2016**, *7*, No. 11580.

(6) Wang, P.; Guo, S.; Wang, H. J.; Chen, K. K.; Zhang, N.; Zhang, Z. M.; Lu, T. B. A Broadband and Strong Visible-Light-Absorbing Photosensitizer Boosts Hydrogen Evolution. *Nat. Commun.* **2019**, *10*, No. 3155.

(7) Zhao, J.; Wu, W.; Sun, J.; Guo, S. Triplet Photosensitizers: From Molecular Design to Applications. *Chem. Soc. Rev.* **2013**, *42*, 5323−5351.

(8) Chen, H.; Zeng, X.; Tham, H. P.; Phua, S. Z. F.; Cheng, W.; Zeng, W.; Shi, H.; Mei, L.; Zhao, Y. NIR-Light-Activated Combination Therapy with a Precise Ratio of Photosensitizer and Prodrug Using a Host−Guest Strategy. *Angew. Chem., Int. Ed.* **2019**, *58*, 7641−7646.

(9) Gao, J.; Li, J.; Geng, W. C.; Chen, F. Y.; Duan, X.; Zheng, Z.; Ding, D.; Guo, D. S. Biomarker Displacement Activation: A General Host−Guest Strategy for Targeted Phototheranostics in Vivo. *J. Am. Chem. Soc.* **2018**, *140*, 4945−4953.

(10) Kwon, N.; Kim, H.; Li, X.; Yoon, J. Supramolecular Agents for Combination of Photodynamic Therapy and Other Treatments. *Chem. Sci.* **2021**, *12*, 7248−7268.

(11) Li, M.; Shao, Y.; Kim, J. H.; Pu, Z.; Zhao, X.; Huang, H.; Xiong, T.; Kang, Y.; Li, G.; Shao, K.; Fan, J.; Foley, J. W.; Kim, J. S.; Peng, X. Unimolecular Photodynamic O$_2$-Economizer to Overcome Hypoxia Resistance in Phototherapeutics. *J. Am. Chem. Soc.* **2020**, *142*, 5380−5388.

(12) Liu, B.; Jiao, J.; Xu, W.; Zhang, M.; Cui, P.; Guo, Z.; Deng, Y.; Chen, H.; Sun, W. Highly Efficient Far-Red/NIR-Absorbing Neutral Ir(III) Complex Micelles for Potent Photodynamic/Photothermal Therapy. *Adv. Mater.* **2021**, *33*, No. 2100795.

(13) Liu, S.; Li, Y.; Kwok, R. T. K.; Lam, J. W. Y.; Tang, B. Z. Structural and Process Controls of Aiegens for NIR-II Theranostics. *Chem. Sci.* **2021**, *12*, 3427−3436.

(14) Nguyen, V. N.; Yan, Y.; Zhao, J.; Yoon, J. Heavy-Atom-Free Photosensitizers: From Molecular Design to Applications in the Photodynamic Therapy of Cancer. *Acc. Chem. Res.* **2021**, *54*, 207−220.

(15) Sun, C.; Zhang, H.; Yue, L.; Li, S.; Cheng, Q.; Wang, R. Facile Preparation of Cucurbit[6]Uril-Based Polymer Nanocapsules for Targeted Photodynamic Therapy. *ACS Appl. Mater. Interfaces* **2019**, *11*, 22925−22931.

(16) Xue, L.; Shen, Q.; Zhang, T.; Fan, Y.; Xu, X.; Shao, J.; Yang, D.; Zhao, W.; Dong, X.; Mou, X. Fluorescence Resonance Energy Transfer Enhanced Photothermal and Photodynamic Antibacterial Therapy Post a Single Injection. *Mater. Chem. Front.* **2021**, *5*, 6061−6070.

(17) Yuan, B.; Wu, H.; Wang, H.; Tang, B.; Xu, J. F.; Zhang, X. A Self-Degradable Supramolecular Photosensitizer with High Photodynamic Therapeutic Efficiency and Improved Safety. *Angew. Chem., Int. Ed.* **2021**, *60*, 706−710.

(18) Zhang, Y.; Ma, S.; Liu, X.; Xu, Y.; Zhao, J.; Si, X.; Li, H.; Huang, Z.; Wang, Z.; Tang, Z.; Song, W.; Chen, X. Supramolecular Assembled Programmable Nanomedicine as in Situ Cancer Vaccine for Cancer Immunotherapy. *Adv. Mater.* **2021**, *33*, No. 2007293.

(19) Zhu, H.; Wang, H.; Shi, B.; Shangguan, L.; Tong, W.; Yu, G.; Mao, Z.; Huang, F. Supramolecular Peptide Constructed by Molecular Lego Allowing Programmable Self-Assembly for Photodynamic Therapy. *Nat. Commun.* **2019**, *10*, No. 2412.

(20) Bittner, E. R.; Lankevich, V.; Gelinas, S.; Rao, A.; Ginger, D. A.; Friend, R. H. How Disorder Controls the Kinetics of Triplet Charge Recombination in Semiconducting Organic Polymer Photovoltaics. *Phys. Chem. Chem. Phys.* **2014**, *16*, 20321−20328.

(21) Qin, L.; Liu, X.; Zhang, X.; Yu, J.; Yang, L.; Zhao, F.; Huang, M.; Wang, K.; Wu, X.; Li, Y.; Chen, H.; Wang, K.; Xia, J.; Lu, X.; Gao, F.; Yi, Y.; Huang, H. Triplet Acceptors with a D-A Structure and Twisted Conformation for Efficient Organic Solar Cells. *Angew. Chem.* **2020**, *132*, 15153−15159.

(22) Yang, L.; Gu, W.; Lv, L.; Chen, Y.; Yang, Y.; Ye, P.; Wu, J.; Hong, L.; Peng, A.; Huang, H. Triplet Tellurophene-Based Acceptors for Organic Solar Cells. *Angew. Chem., Int. Ed.* **2018**, *57*, 1096−1102.

(23) Bhatia, H.; Dey, S.; Ray, D. Effect of π−π Interactions of Donor Rings on Persistent Room-Temperature Phosphorescence in D$_4$−A Conjugates and Data Security Application. *ACS Omega* **2021**, *6*, 3858−3865.

(24) Liu, Z. Y.; Hu, J. W.; Huang, C. H.; Huang, T. H.; Chen, D. G.; Ho, S. Y.; Chen, K. Y.; Li, E. Y.; Chou, P. T. Sulfur-Based Intramolecular Hydrogen-Bond: Excited-State Hydrogen-Bond on/off Switch with Dual Room-Temperature Phosphorescence. *J. Am. Chem. Soc.* **2019**, *141*, 9885−9894.

(25) Ma, L.; Sun, S.; Ding, B.; Ma, X.; Tian, H. Highly Efficient Room−Temperature Phosphorescence Based on Single−Benzene Structure Molecules and Photoactivated Luminescence with Afterglow. *Adv. Funct. Mater.* **2021**, *31*, No. 2010659.

(26) Nara, M.; Orita, R.; Ishige, R.; Ando, S. White-Light Emission and Tunable Luminescence Colors of Polyimide Copolymers Based on FRET and Room-Temperature Phosphorescence. *ACS Omega* **2020**, *5*, 14831−14841.

(27) Thomas, H.; Fries, F.; Gmelch, M.; Barschneider, T.; Kroll, M.; Vavaleskou, T.; Reineke, S. Purely Organic Microparticles Showing Ultralong Room Temperature Phosphorescence. *ACS Omega* **2021**, *6*, 13087−13093.

(28) Zhang, T.; Ma, X.; Wu, H.; Zhu, L.; Zhao, Y.; Tian, H. Molecular Engineering for Metal-Free Amorphous Materials with Room-Temperature Phosphorescence. *Angew. Chem., Int. Ed.* **2020**, *59*, 11206−11216.

(29) Zhang, Y.; Gao, L.; Zheng, X.; Wang, Z.; Yang, C.; Tang, H.; Qu, L.; Li, Y.; Zhao, Y. Ultraviolet Irradiation-Responsive Dynamic Ultralong Organic Phosphorescence in Polymeric Systems. *Nat. Commun.* **2021**, *12*, No. 2297.

(30) Zhao, W.; He, Z.; Tang, B. Z. Room-Temperature Phosphorescence from Organic Aggregates. *Nat. Rev. Mater.* **2020**, *5*, 869−885.

(31) Fan, C.; Wu, W.; Chruma, J. J.; Zhao, J.; Yang, C. Enhanced Triplet−Triplet Energy Transfer and Upconversion Fluorescence through Host−Guest Complexation. *J. Am. Chem. Soc.* **2016**, *138*, 15405−15412.

(32) Kouno, H.; Ogawa, T.; Amemori, S.; Mahato, P.; Yanai, N.; Kimizuka, N. Triplet Energy Migration-Based Photon Upconversion by Amphiphilic Molecular Assemblies in Aerated Water. *Chem. Sci.* **2016**, *7*, 5224−5229.

(33) Nonat, A.; Chan, C. F.; Liu, T.; Platas-Iglesias, C.; Liu, Z.; Wong, W. T.; Wong, W. K.; Wong, K. L.; Charbonniere, L. J. Room Temperature Molecular Upconversion in Solution. *Nat. Commun.* **2016**, *7*, No. 11978.

(34) Ravetz, B. D.; Pun, A. B.; Churchill, E. M.; Congreve, D. N.; Rovis, T.; Campos, L. M. Photoredox Catalysis Using Infrared Light via Triplet Fusion Upconversion. *Nature* **2019**, *565*, 343−346.

(35) Simon, Y. C.; Weder, C. Low-Power Photon Upconversion through Triplet−Triplet Annihilation in Polymers. *J. Mater. Chem.* **2012**, *22*, 20817−20830.

(36) Singh-Rachford, T. N.; Castellano, F. N. Photon Upconversion Based on Sensitized Triplet−Triplet Annihilation. *Coord. Chem. Rev.* **2010**, *254*, 2560−2573.

(37) Wang, Z.; Hou, Y.; Huo, Z.; Liu, Q.; Xu, W.; Zhao, J. Spatially Confined Photoexcitation with Triplet−Triplet Annihilation Upconversion. *Chem. Commun.* **2021**, *57*, 9044−9047.

(38) Xiao, X.; Tian, W.; Imran, M.; Cao, H.; Zhao, J. Controlling the Triplet States and Their Application in External Stimuli-Responsive Triplet−Triplet−Annihilation Photon Upconversion: From the Perspective of Excited State Photochemistry. *Chem. Soc. Rev.* **2021**, *50*, 9686−9714.

(39) Yang, D.; Han, J.; Liu, M.; Duan, P. Photon Upconverted Circularly Polarized Luminescence via Triplet−Triplet Annihilation. *Adv. Mater.* **2019**, *31*, No. 1805683.

(40) Zhang, C.; Zhao, J.; Wu, S.; Wang, Z.; Wu, W.; Ma, J.; Guo, S.; Huang, L. Intramolecular RET Enhanced Visible Light-Absorbing Bodipy Organic Triplet Photosensitizers and Application in Photooxidation and Triplet−Triplet Annihilation Upconversion. *J. Am. Chem. Soc.* **2013**, *135*, 10566−10578.

(41) Zhou, J.; Liu, Z.; Li, F. Upconversion Nanophosphors for Small-Animal Imaging. *Chem. Soc. Rev.* **2012**, *41*, 1323−1349.

(42) Sun, J.; Zhong, F.; Yi, X.; Zhao, J. Efficient Enhancement of the Visible-Light Absorption of Cyclometalated Ir(III) Complexes Triplet Photosensitizers with Bodipy and Applications in Photooxidation and Triplet−Triplet Annihilation Upconversion. *Inorg. Chem.* **2013**, *52*, 6299−6310.

(43) Ji, S.; Guo, H.; Wu, W.; Wu, W.; Zhao, J. Ruthenium(II) Polyimine-Coumarin Dyad with Non-Emissive ^{3}IL Excited State as Sensitizer for Triplet−Triplet Annihilation Based Upconversion. *Angew. Chem., Int. Ed.* **2011**, *50*, 8283−8286.

(44) Ji, S.; Wu, W.; Wu, W.; Guo, H.; Zhao, J. Ruthenium(II) Polyimine Complexes with a Long-Lived ^{3}IL Excited State or a ^{3}MLCT/^{3}IL Equilibrium: Efficient Triplet Sensitizers for Low-Power Upconversion. *Angew. Chem., Int. Ed.* **2011**, *50*, 1626−1629.

(45) Cui, X.; Zhao, J.; Lou, Z.; Li, S.; Wu, H.; Han, K. L. Switching of the Triplet Excited State of Rhodamine/Naphthaleneimide Dyads: An Experimental and Theoretical Study. *J. Org. Chem.* **2015**, *80*, 568−581.

(46) Huang, L.; Li, Z.; Zhao, Y.; Yang, J.; Yang, Y.; Pendharkar, A. I.; Zhang, Y.; Kelmar, S.; Chen, L.; Wu, W.; Zhao, J.; Han, G. Enhancing Photodynamic Therapy through Resonance Energy Transfer Constructed Near-Infrared Photosensitized Nanoparticles. *Adv. Mater.* **2017**, *29*, No. 1604789.

(47) Dong, Y.; Dick, B.; Zhao, J. Twisted Bodipy Derivative as a Heavy-Atom-Free Triplet Photosensitizer Showing Strong Absorption of Yellow Light, Intersystem Crossing, and a High-Energy Long-Lived Triplet State. *Org. Lett.* **2020**, *22*, 5535−5539.

(48) Hou, Y.; Liu, Q.; Zhao, J. An Exceptionally Long-Lived Triplet State of Red Light-Absorbing Compact Phenothiazine-StyrylBodipy Electron Donor/Acceptor Dyads: A Better Alternative to the Heavy Atom-Effect? *Chem. Commun.* **2020**, *56*, 1721−1724.

(49) Liu, D.; El-Zohry, A. M.; Taddei, M.; Matt, C.; Bussotti, L.; Wang, Z.; Zhao, J.; Mohammed, O. F.; Di Donato, M.; Weber, S. Long-Lived Charge-Transfer State Induced by Spin-Orbit Charge Transfer Intersystem Crossing (SOCT-ISC) in a Compact Spiro Electron Donor/Acceptor Dyad. *Angew. Chem., Int. Ed.* **2020**, *59*, 11591−11599.

(50) Wang, Z.; Huang, L.; Yan, Y.; El-Zohry, A. M.; Toffoletti, A.; Zhao, J.; Barbon, A.; Dick, B.; Mohammed, O. F.; Han, G. Elucidation

of the Intersystem Crossing Mechanism in a Helical Bodipy for Low-Dose Photodynamic Therapy. *Angew. Chem., Int. Ed.* **2020**, *59*, 16114−16121.

(51) Sun, J.; Dai, Y.; Hou, Y.; Wu, Q.; Ma, L.; Zhao, J.; Wang, B. Weakened Triplet−Triplet Annihilation of Diiodo-Bodipy Moieties without Influence on Their Intrinsic Triplet Lifetimes in Diiodo-Bodipy-Functionalized Pillar[5]Arenes. *J. Phys. Chem. A* **2021**, *125*, 2344−2355.

(52) Wu, W.; Guo, H.; Wu, W.; Ji, S.; Zhao, J. Organic Triplet Sensitizer Library Derived from a Single Chromophore (Bodipy) with Long-Lived Triplet Excited State for Triplet−Triplet Annihilation Based Upconversion. *J. Org. Chem.* **2011**, *76*, 7056−7064.

(53) Wang, F.; Han, C.; He, C.; Zhou, Q.; Zhang, J.; Wang, C.; Li, N.; Huang, F. Self-Sorting Organization of Two Heteroditopic Monomers to Supramolecular Alternating Copolymers. *J. Am. Chem. Soc.* **2008**, *130*, 11254−11255.

(54) Ashton, P. R.; Fyfe, M. C. T.; Glink, P. T.; Menzer, S.; Stoddart, J. F.; White, A. J. P.; Williams, D. J. Multiply Stranded and Multiply Encircled Pseudorotaxanes. *J. Am. Chem. Soc.* **1997**, *119*, 12514−12524.

(55) Dong, S.; Zheng, B.; Xu, D.; Yan, X.; Zhang, M.; Huang, F. A Crown Ether Appended Super Gelator with Multiple Stimulus Responsiveness. *Adv. Mater.* **2012**, *24*, 3191−3195.

(56) Huang, F.; Scherman, O. A. Supramolecular Polymers. *Chem. Soc. Rev.* **2012**, *41*, 5879−5880.

(57) Yan, X.; Xu, D.; Chi, X.; Chen, J.; Dong, S.; Ding, X.; Yu, Y.; Huang, F. A Multiresponsive, Shape-Persistent, and Elastic Supramolecular Polymer Network Gel Constructed by Orthogonal Self-Assembly. *Adv. Mater.* **2012**, *24*, 362−369.

(58) Li, J.; Yim, D.; Jang, W. D.; Yoon, J. Recent Progress in the Design and Applications of Fluorescence Probes Containing Crown Ethers. *Chem. Soc. Rev.* **2017**, *46*, 2437−2458.

(59) Wu, D.; Sedgwick, A. C.; Gunnlaugsson, T.; Akkaya, E. U.; Yoon, J.; James, T. D. Fluorescent Chemosensors: The Past, Present and Future. *Chem. Soc. Rev.* **2017**, *46*, 7105−7123.

(60) Weißenstein, A.; Saha-Moller, C. R.; Wurthner, F. Optical Sensing of Aromatic Amino Acids and Dipeptides by a Crown-Ether-Functionalized Perylene Bisimide Fluorophore. *Chem. − Eur. J.* **2018**, *24*, 8009−8016.

(61) Erbas-Cakmak, S.; Kolemen, S.; Sedgwick, A. C.; Gunnlaugsson, T.; James, T. D.; Yoon, J.; Akkaya, E. U. Molecular Logic Gates: The Past, Present and Future. *Chem. Soc. Rev.* **2018**, *47*, 2228−2248.

(62) Zhu, X.; Chen, C. A Highly Efficient Approach to [4]Pseudocatenanes by Threefold Metathesis Reactions of a Triptycene-Based Tris[2]pseudorotaxane. *J. Am. Chem. Soc.* **2005**, *127*, 13158−13159.

(63) Amano, S.; Fielden, S. D. P.; Leigh, D. A. A Catalysis-Driven Artificial Molecular Pump. *Nature* **2021**, *594*, 529−534.

(64) Ma, X.; Zhang, J.; Cao, J.; Yao, X.; Cao, T.; Gong, Y.; Zhao, C.; Tian, H. A Room Temperature Phosphorescence Encoding [2]-Rotaxane Molecular Shuttle. *Chem. Sci.* **2016**, *7*, 4582−4588.

(65) Mao, M.; Zhang, X. K.; Xu, T. Y.; Wang, X. D.; Rao, S. J.; Liu, Y.; Qu, D. H.; Tian, H. Towards a Hexa-Branched [7]Rotaxane from a [3]Rotaxane Via a [2+2+2] Alkyne Cyclotrimerization Process. *Chem. Commun.* **2019**, *55*, 3525−3528.

(66) Rao, S. J.; Zhang, Q.; Mei, J.; Ye, X. H.; Gao, C.; Wang, Q. C.; Qu, D. H.; Tian, H. One-Pot Synthesis of Hetero[6]Rotaxane Bearing Three Different Kinds of Macrocycle through a Self-Sorting Process. *Chem. Sci.* **2017**, *8*, 6777−6783.

(67) Tian, C.; Fielden, S. D. P.; Whitehead, G. F. S.; Vitorica-Yrezabal, I. J.; Leigh, D. A. Weak Functional Group Interactions Revealed through Metal-Free Active Template Rotaxane Synthesis. *Nat. Commun.* **2020**, *11*, No. 744.

(68) Chen, S.; Wang, Y.; Nie, T.; Bao, C.; Wang, C.; Xu, T.; Lin, Q.; Qu, D.; Gong, X.; Yang, Y.; Zhu, L.; Tian, H. An Artificial Molecular Shuttle Operates in Lipid Bilayers for Ion Transport. *J. Am. Chem. Soc.* **2018**, *140*, 17992−17998.

(69) Pedersen, C. J. The Discovery of Crown Ethers (Noble Lecture). *Angew. Chem., Int. Ed.* **1988**, *27*, 1021−1027.

(70) Cram, D. J. The Design of Molecular Hosts, Guests, and Their Complexes (Nobel Lecture). *Angew. Chem., Int. Ed.* **1988**, *27*, 1009−1112.

(71) Lehn, J.-M. Supramolecular Chemistry−Scope and Perspectives Molecules, Supermolecules, and Molecular Devices (Nobel Lecture). *Angew. Chem., Int. Ed.* **1988**, *27*, 89−112.

(72) Ozlem, S.; Akkaya, E. U. Thinking Outside the Silicon Box Molecular and Logic as an Additional Layer of Selectivity in Singlet Oxygen Generation for Photodynamic Therapy. *J. Am. Chem. Soc.* **2009**, *131*, 48−49.

(73) Kim, H. J.; Kim, S. H.; Kim, J. H.; Lee, E.-H.; Kim, K.-W.; Kim, J. S. BODIPY Appended Crown Ethers: Selective Fluorescence Changes for Hg^{2+} Binding. *Bull. Korean Chem. Soc.* **2008**, *29*, 1831−1834.

(74) Stephens, P. J.; Devlin, F. J.; Chabalowski, C. F.; Frisch, M. J. Ab Initio Calculation of Vibrational Absorption and Circular Dichroism Spectra Using Density Functional Force Fields. *J. Phys. Chem. A* **1994**, *98*, 11623−11627.

(75) Hariharan, P. C.; Pople, J. A. The Influence of Polarization Functions on Molecular Orbital Hydrogenation Energies. *Theor. Chim. Acta* **1973**, *28*, 213−222.

(76) Frisch, M. J.; Trucks, G. W.; Schlegel, H. B.; Scuseria, G. E.; Robb, M. A.; Cheeseman, J. R.; Scalmani, G.; Barone, V.; Mennucci, B.; Petersson, G. A. et al. *Gaussian 09*, revision D.01; Gaussian Inc.: Wallingford CT, 2013.

(77) Wang, Z.; Sukhanov, A. A.; Toffoletti, A.; Sadiq, F.; Zhao, J.; Barbon, A.; Voronkova, V. K.; Dick, B. Insights into the Efficient Intersystem Crossing of Bodipy-Anthracene Compact Dyads with Steady-State and Time-Resolved Optical/Magnetic Spectroscopies and Observation of the Delayed Fluorescence. *J. Phys. Chem. C* **2019**, *123*, 265−274.

(78) El-Khouly, M. E.; Amin, A. N.; Zandler, M. E.; Fukuzumi, S.; D'Souza, F. Near-IR Excitation Transfer and Electron Transfer in a BF_2-Chelated Dipyrromethane-Azadipyrromethane Dyad and Triad. *Chem. − Eur. J.* **2012**, *18*, 5239−5247.